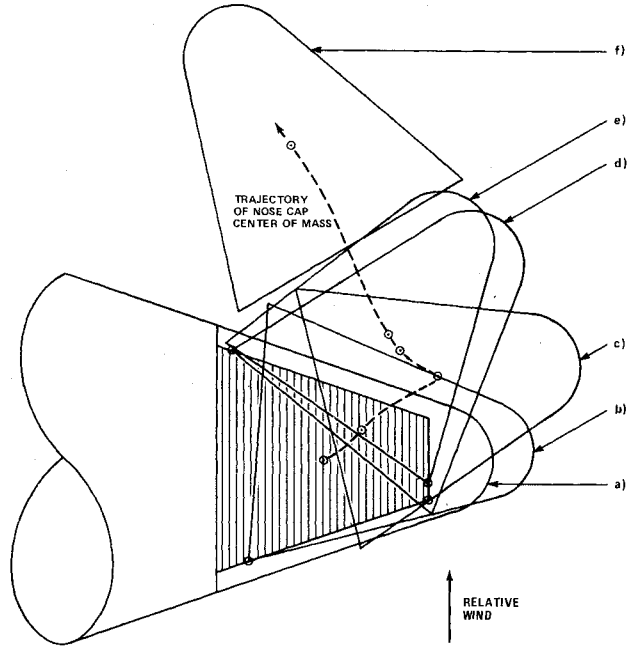

Fig. 2 Nose cap motion relative to rocket during successive impacts.

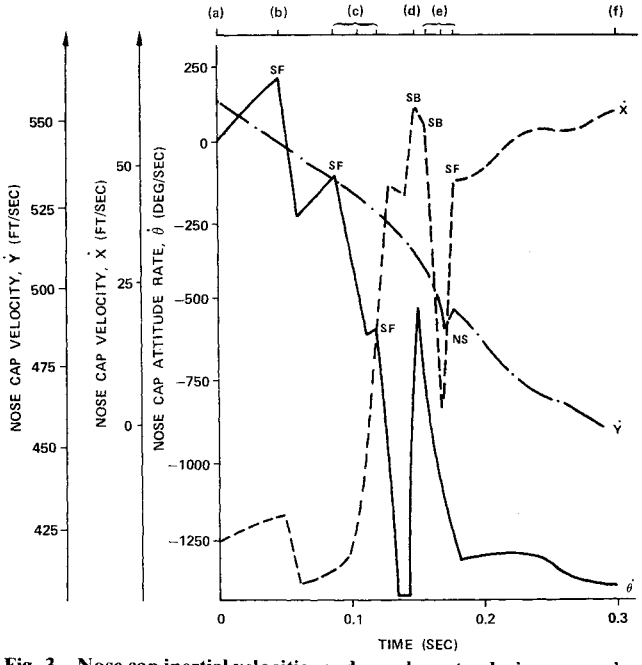

Fig. 3 Nose cap inertial velocities and angular rates during successive impacts.

ward" and "backward" is related to the fact that the tangential component of separation velocity is opposite in sense to tangential impulse $N_2 n_2$. Thus Eqs. (7) and (8) hold only if

$$N_2[V^{Q/P}(t_+)\cdot n_2] < 0 \tag{9}$$

Analysis of an actual impact is started using Eqs. (2, 4, and 5). If the test in Eq. (6) fails, Eq. (5) is replaced by Eq. (7) and the test in Eq. (9) is applied to the resulting solution. If this too fails, the only possible solution is that given by Eqs. (2, 4, and 8).

Impact Detection

To use the preceding equations appropriately, positions of both bodies and their velocities at the exact instant of impact are required. Usually free flight equations of both bodies are integrated forward in time from a nonimpact configuration until time (t) at which an interpenetration of their geometric boundaries is indicated. Noting the penetration depth d of the point Q normal to the surface, a time interval $\Delta t = t - t_-$ is calculated from

$$d = -V^{Q/Q'}\cdot n_1 \Delta t - a^{Q/Q'} n_1 (\Delta t)^2/2 \tag{10}$$

where $V^{Q/Q'}$, $a^{Q/Q'}$ are the relative velocity and acceleration of Q with respect to Q', an image point of Q (after penetration) in the rocket R. Position and velocity of the impact point Q, just before impact, are obtained by backward integration as

$$q_r(t_-) = q_r(t) - \dot{q}_r(t)\Delta t - \ddot{q}_r(t)[(\Delta t)^2/2 \tag{11}$$

$$\dot{q}_r(t_-) = \dot{q}_r(t) - \ddot{q}_r(t)\Delta t \tag{12}$$

The quantities $\dot{q}_r$, $\dot{q}_r$ are obtained from the equation of motion and its first integral.

Steady-state aerodynamic coefficients based on unpublished wind tunnel test data on the nose cap (obtained from NASA Marshall Space Flight Center) were used in the equations of motion before and after impact. Consideration of the dynamic coefficients would be advisable because of the wide variation in angle of attack and velocities of the nose cap. Also, use of the interference aerodynamics data would be highly desirable.

Simulation Results

A typical case of separation with multiple impacts was obtained for the nose cap ejected at a velocity of 20 fps normal to the direction of the air flow. Coefficients of friction ($\mu = 0.25$), and restitution ($e = 0.85$) were selected. Seven successive impacts were detected and simulated. The motion of the nose cap relative to the rocket is shown on Fig. 2, where successive configurations are indicated. At separation, configuration (a), the cap takes a nose down motion relative to the rocket and impacts the parachute pack in (b). This impact causes the cap to bounce backwards and collide in diverse configurations (c-e) before going in free flight, (f). Inertial velocities and nose cap angular rates are plotted vs time on Fig. 3. All three types of impacts, slip forward (SF), slip backward (SB), and no slip (NS) actually happened in this case and are identified in this figure. The present analysis is applicable to impacts involving three-dimensional motion; the problem of locating the impact points, however, then becomes extremely cumbersome.

Reference

[1] Kane, T.R., *Dynamics*, Holt, Rinehart and Winston, New York, 1968, pp. 222-235.

Effects of Nosetip Shape Change on Re-entry Vehicle Dispersion

A. M. Morrison*
Naval Surface Weapons Center, Silver Spring, Md.

Nomenclature

C_A = axial force coefficient
C_D = drag coefficient

Received May 8, 1975; revision received July 10, 1975. Sponsored by the Naval Sea Systems Command under the Aeroballistic Re-entry Technology Program

Index categories: Entry Vehicle Mission Studies and Flight Mechanics; LV/M Aerodynamics.

*Aerospace Engineer, Applied Aerodynamics Division, White Oak Laboratory. Member AIAA.

C_N = normal force coefficient
g = acceleration of gravity (fps $^{-2}$)

H = geopotential altitude $(1/g_0 \int_0^h g dh)$

K_{LAM} = effective surface roughness height (in.)
M_∞ = freestream Mach number
r = radius (in.)
r_B = base radius (ft)
r_n = nose radius (ft)
S = area (ft^2)
V_E = entry velocity (kfps)
W = weight (lb)
X = axial length measured from prere-entry nosetip (in.)
X_{CP} = normalized center-of-pressure location

X_{STAG} = stagnation point recession (in.)
α = angle of attack (deg)
β = angle of sideslip (deg)
θ_c = cone half angle (deg)
γ_e = re-entry flight path angle (deg)
κ_B = modified ballistic coefficient $-C_D \rho_0 S \lambda g / 2W \sin\gamma_e$
ρ = density (lb sec^2 ft^{-4})
λ = constant $\approx$23800 (ft)

Subscript

o = sea-level condition

THIS Note will discuss the results of a recent analytic investigation whose objective was to assess the effects of nosetip shape change upon the dispersion and loading of re-entry vehicles. The simulation technique utilized is discussed and results are presented which indicate that small variations in nosetip shape can lead to significant dispersion.

This approach relies on analytic trajectory simulation. The analysis begins by compiling the metrological characteristics of the configuration of interest. These characteristics are used in conjunction with a three-dimensional inviscid, finite-difference, flowfield code to obtain pressure distributions over a sphere-cone configuration as a function of angle of attack and Mach number. The pressure distributions are integrated to obtain the normal force coefficient, C_N, the axial force coefficient, C_A and the location of the center of pressure, X_{CP}. The drag coefficient of the sphere alone, $C_{D_{SPHERE}}$, is also obtained as a result of this operation.

Concurrent with this computation, a two-degree-of-freedom trajectory simulator provides an altitude-velocity history for the entry velocity and flight path angle of interest. This information is used to start a nosetip shape-change code[1] which provides an altitude-nosetip shape history. Newtonian methods are then applied to the nosetips determined to obtain a drag coefficient history. The nosetip drag history and the results of the inviscid flowfield calculation are used as input for a nosetip shape-aerodynamic characteristic similarity expression. This expression is suggested by blast wave analysis[2] and accounts for the pressure field variation induced by the ablative nosetip shape. The similarity expression,

$$\left[\frac{\text{LENGTH}}{\text{RADIUS}_{nose}}\right]_{\substack{\text{EQUIVALENT}\\ \text{SPHERE CONE}}} = \left[\frac{C_{D\ \text{sphere}}}{C_{D_{NOSE}}}\right]^{1/2} \times \left[\frac{\text{LENGTH}}{\text{SHOULDER HEIGHT}}\right]_{\substack{\text{ABLATED}\\ \text{CONFIGURATION}}}$$

has now been verified by numerous wind-tunnel tests considering spherical, conical, and ablative nosetip geometries.

Ablation nosetip drag effects are scaled as the difference between the ablated nosetip drag coefficient and a pure sphere drag coefficient multiplied by the nosetip-to-base-radius ratio.

The altitude-nosetip shape history is also used as input to a nosetip shape-nosetip normal force correlation.[3] This correlation is shown in Fig. 1. The nosetip normal force, determined from the analysis of a series of free-flight tests, is plotted against the recession of the stagnation point normalized by the nosetip radius. Two curves were correlated in the analysis representative of an average and worst bound for nosetip normal force for the cases considered. Nine free-flight

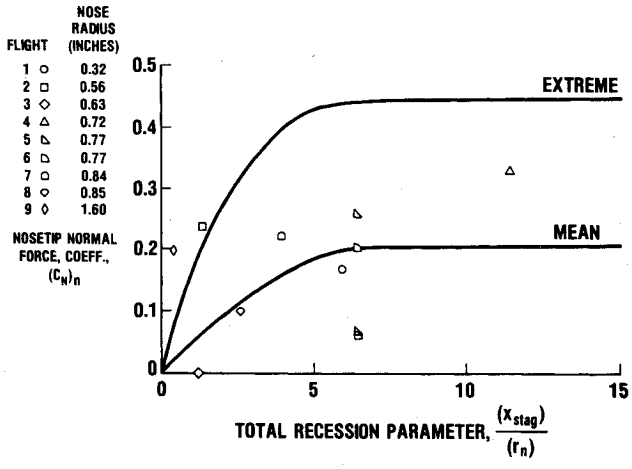

Fig. 1 Nosetip normal force.

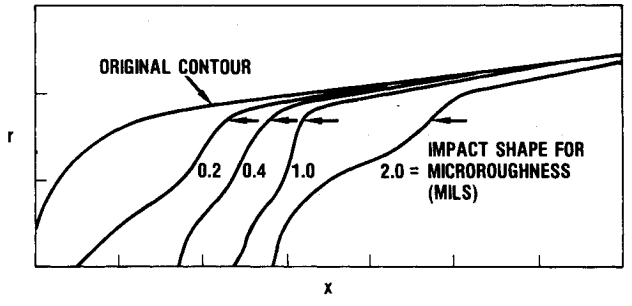

Fig. 2 Impact nosetip shape.

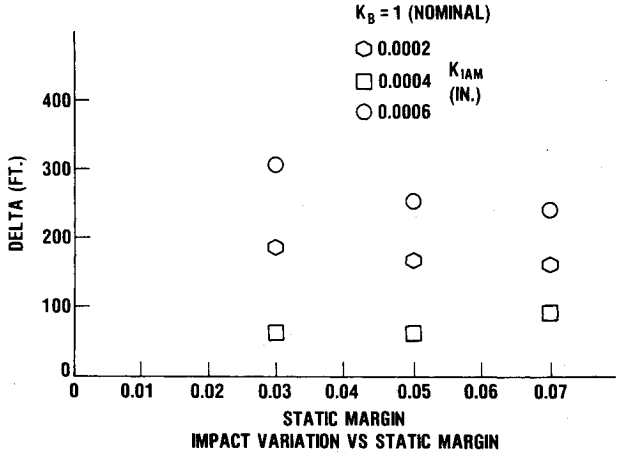

Fig. 3 Nosetip shape sensitivity.

points are represented by the data symbols superimposed on the correlation. None of the free-flight data contained in Fig. 1 were used in the original correlation. These data are for a different nosetip material and a different range of nosetip radii than were considered in the correlation. The correlation appears to be useful even though a nosetip material other than that of the data base is being considered. The correlation represents the alternate material in that the data generally fall into the regimes indicated by the correlation. The scaling with nosetip radius, however, appears to result in an underprediction of nosetip normal force as the flight 9 result of Fig. 1 indicates. The present study considers large radii nosetips and thus the values of nosetip normal force determined may be smaller than would be expected. Further comparisons indicate a need for continuing work in extending this type of correlation to the general case.

All of the information compiled thus far is then used as input for a six-degree-of-freedom, modular, trajectory simulator. Variations in the aerodynamic, material, metrological, and launch conditions may then be investigated using sensitivity techniques. The trajectory simulator and the previously mentioned analytic techniques have been used to simulate conditions for which flight test data is available. Within the limitations of the technique, excellent agreement has been noted between simulated parameters and parameters determined from the flight test data. Such agreement provides further confidence in the methodology.

In order to assess the effects of nosetip shape change upon dispersion, surface roughness heights of two-tenths, four-tenths, and six-tenths of a mil were used to influence the boundary-layer transition criterion in the nosetip shape-change code, thus generating different nosetip shape-change histories. The use of a surface roughness parameter to influence shape change has been investigated and found useful.[4]

Typical impact shapes generated for a range of surface roughness parameter values are given in Fig. 2. Numerous trajectory simulations were made using the generated nosetip shape histories. Representative results of this study are shown in Fig. 3, where impact variation distance for a blunted sphere cone ($R_n/R_B > 0.2$), relative to a nominal, nonablating, seven-percent static-margin sphere-cone trajectory, is plotted vs static margin. Small lift-generated variations occur with static margin for any nosetip history.

The very significant result of this analysis is indicated by the impact variations on the order of 250 ft over the small nosetip shape uncertainty regime indicated for each static margin. From this plot it is concluded that nosetip shape changes significantly affect re-entry vehicle flight performance and can lead to significant impact coordinate variations. The variations presented are due to both lift and drag. Analysis at the seven-percent static margin point shows drag contributing 65% of the impact variation while lift contributes 35%. The variation of surface roughness, shape-generated, impact variation factor is not monotonic because ablative nosetip drag effects may either increase or decrease the blast wave statement (downstream) determined value at various points over the re-entry trajectory. Nosetip shape-change effects are still being analyzed and improvements are being made to simulation techniques.

References

[1] "User's Manual Steady-State Analysis of Ablating Nose Tips—SAANT," UM-73-38, Aerotherm Div., Acurex corp., Mountain View, Calif., Sept. 1973.

[2] Chernyi, G. C., *Introduction to Hypersonic Flow*, Academic Press, New York and London, 1961, pp. 201-234.

[3] Crenshaw, P. J., "Asymmetric Nosetip Transition Effects on Re-Entry Vehicle Trim, Nosetip Shape and Aerodynamics," submitted for publication in *Journal of Spacecraft and Rockets*, 1975.

[4] Welsh, W. E. Jr., "Shape and Surface Roughness Effects on Nosetip Ablation," *AIAA Journal*, Vol. 8, Nov. 1970, pp. 1983-1989.

Evaluation of Boron/Aluminum Tubes in Compression

A. C. Knoell*
Jet Propulsion Laboratory, Pasadena, Calif.

Introduction

CONSIDERABLE attention has recently been given to the development and application of boron/aluminum k/Al) composite material to aircraft[1,2] and spacecraft[3-5] structures. The results of these investigations and others have shown that B/Al offers the potential of improved structural performance at reduced weight when compared to conventional metal counterpart structures. Furthermore, these investigations have also indicated that such improved performance can be confidently and economically gained as a result of improved fabrication techniques and more widespread usage of the material.

Using these results, a brief analytical and experimental investigation was performed to determine the compressive behavior of B/Al tubes. The investigation consisted of determining the full scale column and local crippling strengths of six B/Al tubes. The purpose of the investigation was to gain hardware experience in a limited evaluation of the material for application to spacecraft truss structures. It was recognized that the results of this investigation could also be coupled with other available analytical and experimental data on B/Al, thereby contributing at least in a small manner to an expanded data base of the material. This Note presents the results of that investigation.

Specimen Description

All tubes used in the investigation were fabricated of unidirectional B/Al aligned parallel to the long axis of the tubes with integrally diffusion-bonded titanium end collars. The fiber volume fraction ranged from 47 to 50%. Fiber bend tests performed on leached-out filaments of the material indicated a fiber strength in excess of 500,000 psi.

After fabrication, all tubes were ultrasonically inspected by a through transmission technique. All tubes gave excellent indications of tube/collar bonding. The tubes were also inspected for physical defects; none were observed except for minor localized overetching of one specimen.

The tubes consisted of 3- and 4-ply laminates and were nominally 1.70 in. in diameter by 36 in. long. The specific physical characteristics of the tubes are summarized in Table 1.

Experimental Procedure

All tubes were tested in static compression at a loading rate of approximately 1800 lbf/min at room temperature under ambient conditions. Male end-fitting attachments were used to stabilize the column against lateral motion. A continuous recording of load vs displacement was made for all test specimens. In the case of specimen S/N-1, which was in-

Submitted May 7, 1975; presented as Paper 75-789 at the AIAA/ASME/SAE 16th Structures, Structural Dynamics, and Materials Conference, Denver, Colorado, May 27-29, 1975; revision received June 12, 1975. This work was supported under NASA Contract NAS 7-100. Organizations that contributed were NASA-JSC, Rockwell International Space Division, and General Dynamics Convair Division; W. Jensen and B. Montgomery of JPL conducted the experiments and E. Robinson, formerly of JPL, developed the early arrangements for the program.

Index categories: Materials, Properties of; Structural Composite Materials (including Coatings); Structural Stability Analysis.

*Member of Technical Staff. Associate Fellow AIAA.